Early View publication on wileyonlinelibrary.com
(issue and page numbers not yet assigned;
citable using Digital Object Identifier – DOI)

ZAMM · Z. Angew. Math. Mech., 1 – 12 (2012) / **DOI** 10.1002/zamm.201200035

Modelling strain localization by cohesive/overlapping zones in tension/compression: Brittleness size effects and scaling in material properties

Alberto Carpinteri* **and Marco Paggi** **

Politecnico di Torino, Department of Structural, Geotechnical and Building Engineering, Corso Duca degli Abruzzi 24, 10129 Torino, Italy

Received 22 February 2012, accepted 22 April 2012
Published online 11 June 2012

Key words Cohesive crack model, overlapping crack model, fractal cohesive crack model.

The present paper is a state-of-the-art review of the research carried out at the Politecnico di Torino during the last two decades on the modelling of strain localization. Introducing the elementary cohesive/overlapping models in tension/compression, it will be shown that it is possible to get a deep insight into the ductile-to-brittle transition and into the scaling of the material properties usually detected when testing quasi-brittle material specimens or structures at different size-scales.

1 Introduction

Quasi-brittle materials in tension exhibit strain softening, i.e., a negative slope in the stress-deformation diagram, due to microcracking and localization of the deformation in a narrow band, where energy dissipation takes place.

From the Continuum Mechanics viewpoint, strain softening represents a violation of the Drucker's Postulate [1]. As a consequence, the following phenomena may occur: (i) loss of stability in the controlled load condition (snap-through); (ii) loss of stability in the controlled displacement condition (snap-back). From the historical point of view, such forms of instability were formerly recognized in the post-critical behaviour of shell buckling problems. In the pioneering papers by von Kármán and Tsien [2, 3], the initial geometrical imperfections were found to be responsible for the transition from snap-back to softening branches after the bifurcation point in the load-deflection curves of imperfection-sensitive axially compressed cylinders at large displacements.

The cohesive crack model is able to describe materials that exhibit a strain-softening type behaviour. Dugdale [4] firstly postulated the existence of uniform tractions equal to the yield stress transmitted through a narrow yield zone in front of a crack in elastic-perfectly plastic materials. A detailed analysis of the spread of such a plastic zone was then proposed by Bilby, Cottrell, and Swinden [5]. Independently, Barenblatt [6] proposed the concept of cohesive forces to model the effect of interatomic forces in polycrystals. It is also important to recall that Rice [7] devoted a section of his fundamental paper on the path independent integral to the analysis of the Barenblatt-Dugdale crack model. On the other hand, to the knowledge of the present authors, Smith [8] firstly used the terminology *Cohesive Zone Model* in 1974, which then received a great favour from the scientific Community.

Subsequently, Hillerborg and coworkers [9, 10] proposed the *Fictitious Crack Model* for the study of the nonlinear mechanical behaviour of concrete. More recently, the *Cohesive Crack Model* terminology was introduced by Carpinteri [11–15] when snap-back branches may be captured. This terminology has become very popular and has been used by a number of researchers (for instance, see [16, 17], among others). Advantages and limitations of this approach have been extensively reviewed in [18].

The basic assumption underlying this model is the formation, as an extension of the real crack, of a fictitious crack, referred to also as the *process zone*, where the material, albeit damaged, is still able to transfer stresses. The crack is assumed to propagate when the stress at the crack tip reaches the tensile strength, σ_u. When the crack opens, the stress is not assumed to fall to zero at once, but to decrease gently with increasing crack width, w, until a critical displacement is reached and the interaction vanishes. The amount of energy absorbed per unit crack area is referred to as *fracture energy*, and represents the area under the stress-displacement curve. This modelling requires the use of a pair of constitutive laws:

* E-mail: alberto.carpinteri@polito.it
** Corresponding author E-mail: marco.paggi@polito.it, Phone: +39 011 090 4910, Fax: +39 011 090 4899

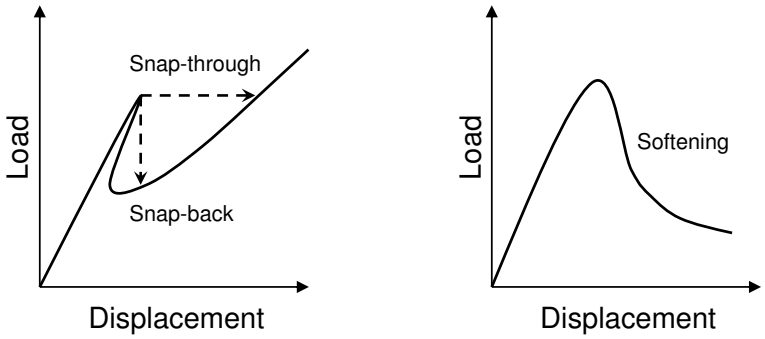

Fig. 1 Post-peak mechanical responses showing snap-back, snap-through or softening branches.

a stress-strain linear-elastic relationship for the undamaged material, and a softening stress-crack opening curve for the damaged material.

From the computational point of view, this approach has demonstrated to be very attractive, since it can be implemented in the finite element method eliminating the stress-singularity at the crack tip typical of Linear Elastic Fracture Mechanics (LEFM), and it permits to avoid the effects of mesh sensitivity [19]. Since 1984, Carpinteri and coworkers have shown that the cohesive crack model can be used for the analysis of stability of the mechanical response of quasi-brittle material specimens or structures, demonstrating that the brittle behaviour and the LEFM critical condition are represented by the occurrence of post-peak softening branches with positive slopes, leading to catastrophic snap-back instabilities under displacement control, in close analogy with the behaviour of shell buckling problems [11–15] (see Fig. 1 for a sketch of the post-peak responses). Such an indenting branch is not virtual only if the loading process is controlled by a monotonically increasing function of time, such as the crack length or the displacement discontinuity across the crack [19]. Moreover, a transition from snap-back to softening branches can be observed, leading to a size-scale effect on the brittleness or ductility. In particular, the specimen behaviour is brittle (snap-back) only for low fracture toughness, high tensile strength, and/or large structural sizes. More specifically, the combined effect of all of these parameters can be investigated by using only one single parameter, the energy brittleness number s_E defined in [11].

In close analogy with the cohesive crack model for the description of strain localization in tension, the *Overlapping Crack Model* has been proposed in [20, 21] for the description of the behaviour of quasi-brittle materials in compression, starting from the pioneering paper by Hillerborg [22]. In this case, crushing takes place when the maximum stress in compression reaches the compressive strength, σ_c. After that, damage is described by a fictitious interpenetration of the two portions of the specimen and it represents the localization of the dissipated energy. This approach is suitable for cases where the strain field localizes along a surface. In other cases, where a more distributed damage inside the volume takes place, other approaches based on damage mechanics should be pursued, see [23].

As for the cohesive model in tension, larger is the interpenetration, also referred to as overlapping, lower are the compressive stresses transmitted by the damaged zone. Coupling of this elementary model with the cohesive one permits to realize a unified numerical algorithm able to describe both cracking and crushing growths during loading processes in reinforced concrete (RC) members in bending.

Moreover, in order to explain the size effects upon the parameters of the cohesive crack model (tensile strength, critical displacement, fracture energy), fractal geometry concepts can be applied to the description of the influence of the microstructural disorder [24, 25]. This led to an extension of the cohesive crack model, the so-called *Fractal Cohesive Crack Model* [26], which was proposed and applied to interpret the experimental tensile data from concrete specimens tested over a broad range of scales.

Finally, in the last few years, an extension of these studies has been carried out for the analysis of instability phenomena at the interfaces in heterogeneous materials [27, 28]. Using the finite element method, the following interface mechanical problems have been modelled: (i) debonding of particles in grained materials and study of the related scale effects depending on the grain size [29]; (ii) delamination of the reinforcement layer in retrofitted beams in bending [30], where the process of interface crack propagation results into severe snap-back instabilities; (iii) study of the delamination of layered beams with imperfect interfaces and multiple microdefects [31].

The present paper is organized as follows: in Sect. 2, an overview of the main features of the elementary Cohesive Crack Model are briefly presented and the numerical aspects are discussed. In Sect. 3, the Overlapping Crack Model is introduced and it will be shown that, using this model, it is possible to effectively capture the flexural behaviour of RC beams, by

varying the reinforcement percentage and/or the beam size. Finally, Sect. 4 is devoted to the generalized Fractal (scale-invariant) Cohesive Crack Model, where the effect of microstructural disorder is taken into account according to fractal geometry.

2 Cohesive Crack Model

The Cohesive Crack Model is based on the following assumptions [9, 11]:

- The cohesive fracture zone (plastic or process zone) begins to develop when the maximum principal stress achieves the ultimate tensile strength, σ_u (see Fig. 2a).
- The material in the process zone is partially damaged but still able to transfer stresses. Such stresses are dependent on the crack opening displacement w (see Fig. 2b).

The energy necessary to produce a unit crack surface is given by the area under the $\sigma - w$ diagram in Fig. 2b:

$$\mathcal{G}_F = \int_0^{w_{cr}^t} \sigma \mathrm{d}w = \frac{1}{2}\sigma_u w_{cr}^t. \tag{1}$$

Here, the superscript (t) refers to the material behaviour in tension. The real crack tip is defined as the point where the distance between the crack surfaces is equal to the critical value of the crack opening displacement, w_{cr}^t, and the normal stress vanishes (see Fig. 2b and Fig. 3) On the other hand, the fictitious crack tip is defined as the point where the normal stress attains the maximum value and the crack opening vanishes (Fig. 2b and Fig. 3).

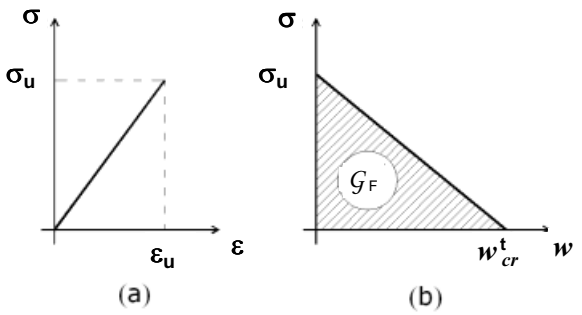

Fig. 2 Constitutive laws of the Cohesive Crack Model: (a) undamaged material, (b) process zone.

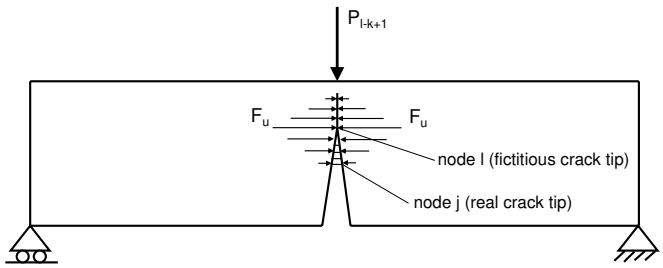

Fig. 3 Cohesive crack configurations at the $(l-k+1)$-th crack growth increment.

Concerning the behaviour of plane concrete elements in Mode I conditions, such as the three point bending test, the crack trajectory is known *a priori* due to geometric symmetry. An extensive series of numerical analyses was carried out from 1984 to 1989 by Carpinteri and coworkers [11–15] based on the cohesive model implemented in the Finite Element Code FRANA (FRacture ANAlysis). A numerical procedure was considered to simulate a loading process where the parameter incremented step by step is the fictitious crack depth. Real (or stress-free) crack depth, external load, and deflection are obtained at each step after an iterative computation. Basically, the closing stresses acting on the crack surfaces are replaced by nodal forces (Figs. 3 and 4). The intensity of these forces depends on the opening of the fictitious crack, w, according to the $\sigma - w$ constitutive law of the material. When the tensile strength σ_u is achieved at the fictitious crack tip, the top node is opened and a cohesive force starts acting across the crack, while the fictitious crack tip moves to the next node.

The coefficients of influence in terms of node openings and deflection are computed by a finite element analysis. At a generic step of the simulation, the crack opening displacements at the n fracture nodes (related to the number of elements m in Fig. 4b as $n = m - 1$) may be expressed as follows:

$$\{w\} = [K]\{F\} + \{C\}P, \tag{2}$$

$\{w\}$ being the vector of the crack opening displacements, $[K]$ the matrix of the coefficients of influence (nodal forces), $\{F\}$ the vector of the nodal forces, $\{C\}$ the vector of the coefficients of influence (external load), and P the external load shown in Fig. 3. The matrix equation (2) constitutes a set of n equation in $(2n + 1)$ unknowns, that is, the nodal displacements,

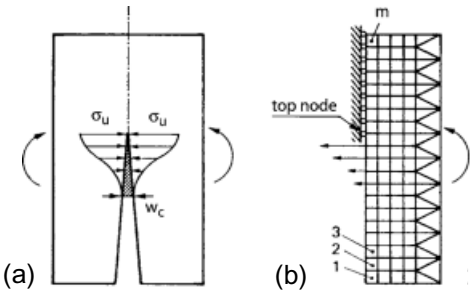

Fig. 4 (a) Stress distribution across the cohesive zone and (b) equivalent nodal forces in the finite element mesh.

the nodal forces and the external force. To solve the problem, $(n+1)$ additional equations have to be considered. When a cohesive zone forms in front of the real crack tip, say between nodes j and l (see Fig. 4), then we have:

$$F_i = 0, \qquad \text{for } i = 1, 2, \ldots, (j-1), \tag{3a}$$

$$F_i = F_u \left(1 - \frac{w_i}{w_{cr}^t}\right), \qquad \text{for } i = j, \ldots, l, \tag{3b}$$

$$w_i = 0, \qquad \text{for } i = l, \ldots, n, \tag{3c}$$

where F_u is the ultimate strength nodal force. Equations (2) and (3) constitute a linear algebraical system of $(2n+1)$ equations in $(2n+1)$ unknowns.

If the load P and the vector $\{F\}$ are found, it is possible to compute the beam deflection, δ:

$$\delta = \{C\}^T \{F\} + D_P P, \tag{4}$$

where D_P is the coefficient of influence for the applied load. The present numerical algorithm simulates a loading process where the controlling parameter is the fictitious crack depth. On the other hand, real (or stress-free) crack depth, external load, and deflection are obtained at each step after an iterative procedure. The program stops with the untying of the node n and, consequently, with the determination of the last pair of values P_n and δ_n. In this way, the complete load-deflection curve is automatically plotted by the computer.

An example of the numerical simulations is shown in the dimensionless load-deflection diagram of Fig. 5 for an unnotched beam made of concrete, $\varepsilon_u = 0.87 \times 10^{-4}$, $\nu = 0.1$, $t = h$, $l = 4h$, and by varying the energy brittleness number $s_E = \mathcal{G}_F/(\sigma_u b)$ [12, 13]. The specimen behaviour is brittle with the appearance of snap-back instabilities for low s_E numbers, i.e., for specimens with low fracture toughness, $\mathcal{G}_F$, high tensile strength, σ_u, and/or large sizes, h. For $s_E \lesssim 10.45 \times 10^{-5}$, the $P-\delta$ curve presents positive slope in the softening branch and a catastrophical event occurs if the loading process is deflection-controlled. Such an indenting branch is not virtual only if the loading process is controlled by a monotonically increasing function of time [32, 33].

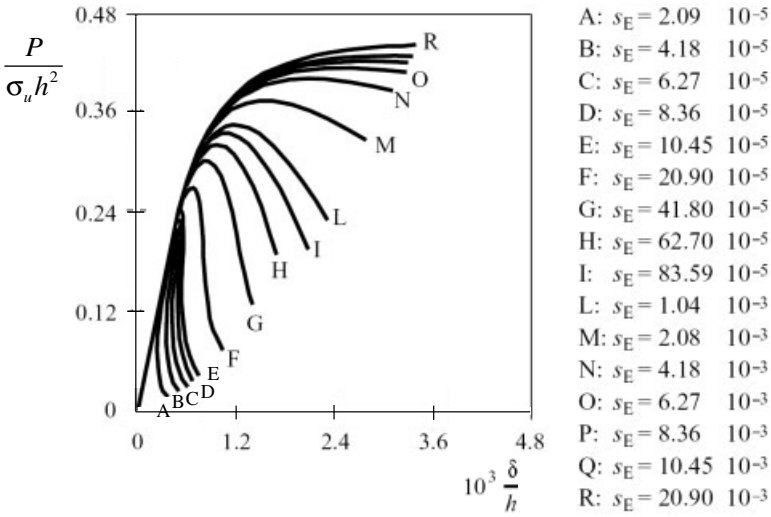

Fig. 5 Dimensionless load versus deflection diagrams by varying the brittleness number s_E, $a_0/h = 0.0$.

Using this model, it is possible to investigate the size-scale effects on tensile strength and fracture toughness. Let us consider the ratio between P_{Cohes} and $P_{U.S.}$, where P_{Cohes} is the maximum loading capacity of initially uncracked specimens directly obtained from Fig. 3 and $P_{U.S.}$ is the maximum load of ultimate strength. The values of this ratio may also be regarded as the ratio of the apparent tensile strength, σ_f, given by the maximum load P_{Cohes}, to the true tensile strength, σ_u. It is evident from Fig. 6 that the results of the cohesive crack model tend to those of the ultimate strength analysis for low s_E values. Therefore, only for comparatively large specimen sizes, the tensile strength σ_u can be obtained as $\sigma_u = \sigma_f$.

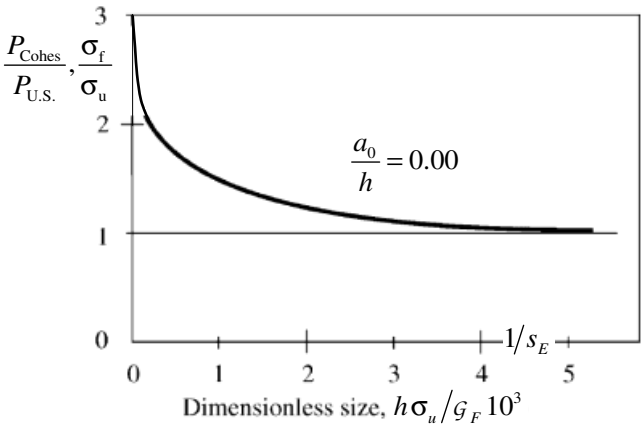

Fig. 6 Decrease in apparent strength by increasing the specimen size.

On the other hand, the values of the ratio $P_{Cohes}/P_{L.E.F.M.}$, where $P_{L.E.F.M}$ is the the maximum load of brittle fracture obtained from the LEFM relations, may also be regarded as the ratio of the fictitious fracture toughness, given by the maximum load P_{Cohes}, to the true fracture toughness considered as a material constant. This ratio is plotted in Fig. 7 as a function of $1/s_E$, and it is evident that, for low s_E numbers, the results of the cohesive crack model tend to those of LEFM. Therefore, in this limit case, the maximum loading capacity can be predicted by applying the simple condition $K_I = K_{IC}$. This also provides an original interpretation to LEFM according to Catastrophe Theory [34], i.e., the Griffith instability for $s_E \to 0$ corresponds to the occurrence of a snap-back instability in the structural response.

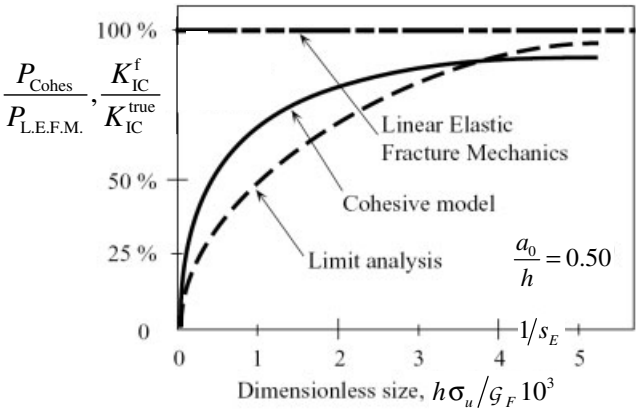

Fig. 7 Increase of fictitious fracture toughness by increasing the specimen size for notched specimens with $a_0/h = 0.50$.

3 Overlapping Crack Model

Also in compression, quasi-brittle materials show the phenomenon of strain localization when the elastic limit is overcome (see Fig. 8).

In close analogy with the Cohesive Crack Model, we can define a pair of constitutive laws in compression. They consist of a linear elastic stress-strain relationship before the achievement of the compression strength, σ_c, and then a softening $\sigma - w$ diagram, where w is a measure of interpenetration (see Fig. 9). The crushing energy (per unit surface), $\mathcal{G}_C$, is the area below the linear softening curve in the $\sigma - w$ diagram and it represents the counterpart of the fracture energy in tension.

The elementary Cohesive and Overlapping Crack Models can be merged into a more complex numerical algorithm for the study of the nonlinear behaviour of RC beams in bending. Following the approach outlined in Sect. 2, a discrete form of the elastic equations governing the mechanical response of the two half-beams can be introduced. The mid-span cross-section of the beam can be subdivided into finite elements by n nodes (see Fig. 10).

In this scheme, cohesive and overlapping stresses are replaced by equivalent nodal forces, F_i, by integrating the corresponding tractions over each element size. Such nodal forces depend on the nodal opening or closing displacements

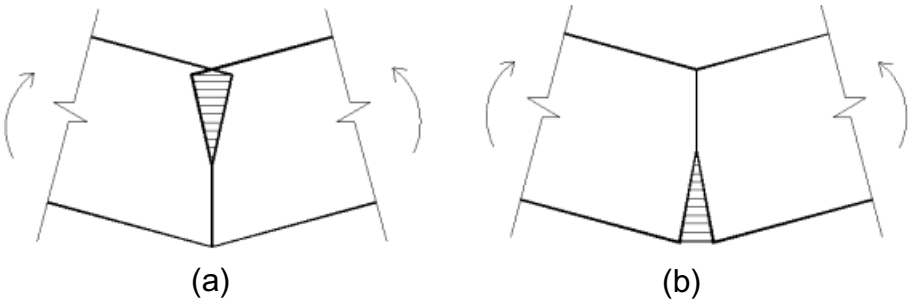

Fig. 8 (a) Compression crushing with overlapping; (b) tensile fracture with cohesive zone.

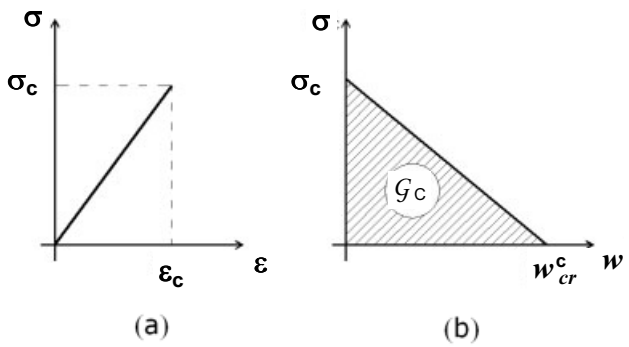

Fig. 9 Constitutive laws of the Overlapping Crack Model: (a) undamaged material, (b) crushing zone.

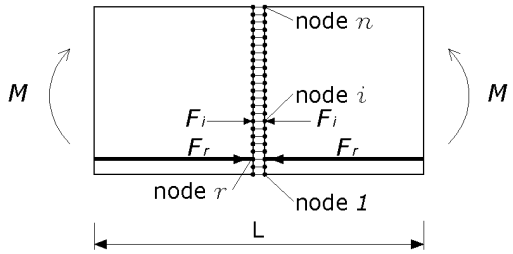

Fig. 10 Finite element nodes along the middle cross-section.

according to the cohesive or overlapping softening laws. Using a mixed approach to deal with the contemporary presence of two crack tips, the vector of the horizontal nodal forces, $\{F\}$, can be computed as follows:

$$\{F\} = [K_w]\{w\} + \{K_M\} M, \tag{5}$$

where $[K_w]$ is the matrix of the coefficients of influence for the nodal displacements, $\{w\}$ is the vector of nodal displacements, $\{K_M\}$ is the vector of the coefficients of transmission for the applied moment and M is the applied moment. Equation (5) permits to analyse the fracturing and crushing process of the mid-span cross-section taking into account the elastic behaviour of the RC member. The reinforcement contribution is also included in the nodal force corresponding to the r-th node. In the generic situation shown in Fig. 11, the following additional equations can be considered:

$$F_i = 0, \qquad \text{for } i = 1, 2, \ldots, (j-1);\ i \neq r, \tag{6a}$$

$$F_i = F_u \left(1 - \frac{w_i^t}{w_{cr}^t}\right), \qquad \text{for } i = j, \ldots, (m-1);\ i \neq r, \tag{6b}$$

$$w_i = 0, \qquad \text{for } i = m, \ldots, p, \tag{6c}$$

$$F_i = F_c \left(1 - \frac{w_i^c}{w_{cr}^c}\right), \qquad \text{for } i = (p+1), \ldots, n, \tag{6d}$$

$$F_r = f(w_r), \qquad \text{for } i = r, \tag{6e}$$

where the superscripts (t) and (c) stand for tension or compression, respectively, whereas F_u and F_c are the ultimate tensile and compresive nodal forces. The index j defines the position of the real crack tip, m the position of fictitious crack tip, p the position of the fictitious overlapping tip and r the node corresponding to the steel reinforcement. The relationship between the closing force exerted by the reinforcing steel and the crack opening at the reinforcement level, i.e., for $i = r$, can be determined on the basis of the bond-slip behaviour of concrete and steel. It is worth noting that, in this framework, it is possible to insert a reinforcement also in compression by introducing a suitable stress-displacement constitutive law in the corresponding node.

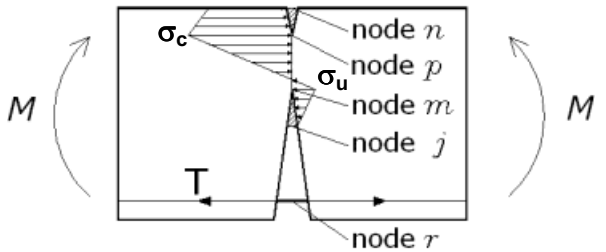

Fig. 11 Stress distribution with a cohesive crack in tension and crushing in compression.

Equations (5) and (6) constitute a linear algebraic system of $(2n)$ equations in $(2n+1)$ unknowns, namely $\{F\}$, $\{w\}$, and M. A possible additional equation can be chosen: we can set either the force in the fictitious crack tip, m, equal to the ultimate tensile force, or the force in the fictitious crushing tip, p, equal to the ultimate compressive force. In the numerical scheme, we choose the situation which is closer to one of these two possible critical conditions. This criterion will ensure the uniqueness of the solution on the basis of physical arguments. The driving parameter of the process is the tip that in the considered step has reached the limit resistance. Only this tip is moved when passing to the next step. The two fictitious tips advance until they converge to the same node. So forth, in order to describe the descending branch of the moment-rotation diagram, the two tips can move together towards the intrados of the beam. As a consequence, the crack in tension closes and the overlapping zone is allowed to extend towards the intrados. This situation is quite commonly observed in over-reinforced beams, where steel yielding does not take place. Finally, at each step of the algorithm, it is possible to calculate the beam rotation, ϑ, as follows:

$$\vartheta = \{D_w\}^{\mathrm{T}} \{w\} + D_M M, \tag{7}$$

where $\{D_w\}$ is the vector of coefficients of influence for the nodal displacements and D_M is the coefficient of influence for the applied moment.

An example of nondimensional moment-rotation diagram that can be obtained using this model is shown in Fig. 12. Considering a reinforcement ratio $\rho = 1.0\%$, the beam depth, h, has been varied from 0.1 m to 2 m, keeping constant and equal to 0.9 the ratio between effective depth, d, and overall depth, h. The slenderness of the tested specimen has been set equal to unity. From the numerical results, it is evident that the structural behaviour becomes more and more brittle by increasing the beam depth. This is very well evidenced by a progressive reduction of the beam rotation at failure. It has to be emphasized that such size-scale effects are not considered in the actual design codes, whereas they have been found in several experimental programmes (see, e.g., [35], among others). Hence, the proposed model is expected to provide a deeper insight into the size-scale effects on the ductility of RC beams in bending.

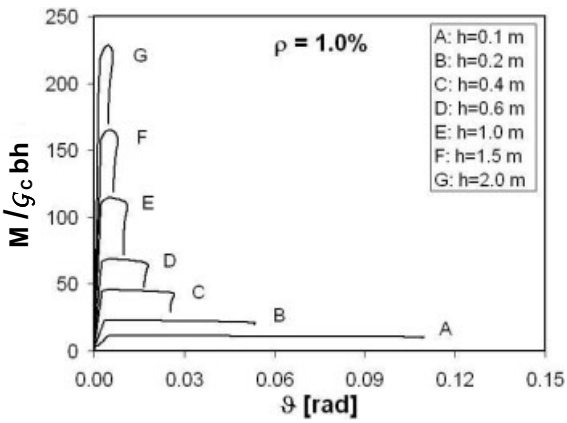

Fig. 12 Nondimensional moment vs. rotation diagrams by varying the beam depth.

4 Fractal Cohesive Crack Model

In order to introduce the Fractal Cohesive Crack Model, we have to consider separately the size effects upon the three parameters characterizing the cohesive law (for more details, the readers are referred to [26]). Hence, let us consider the three fractal domains that are the cause of the size-scale effects on the nominal values of tensile strength, σ_u, critical deformation, ϵ_u, and fracture energy, $\mathcal{G}_F$ (see Fig. 13).

Analyzing a concrete specimen subjected to tension, recent experimental results about porous concrete microstructure [36], as well as a stereological analysis of concrete flaws [37], led us to believe that a consistent modelling of damage

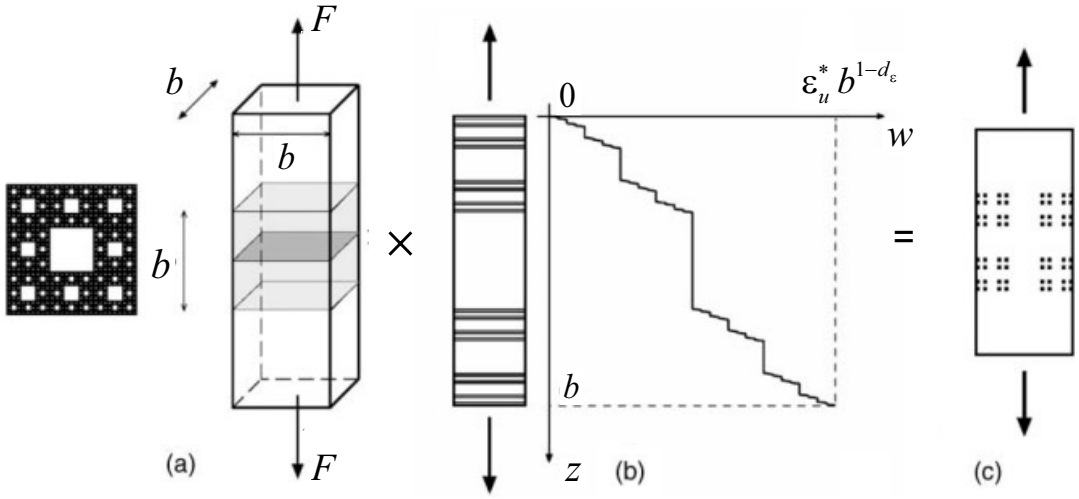

Fig. 13 (a) Fractal localization of the stress upon the resistant cross-section; (b) fractal localization of the strain along the bar length, and (c) fractal energy dissipation inside the damage band.

in concrete can be achieved by assuming that the rarefied resisting sections in correspondence of the critical load can be represented by stochastic lacunar fractal sets with dimension $2 - d_\sigma$, with $d_\sigma \geq 0$ (see Fig. 13a). From fractal geometry, we know that the area of lacunar sets is scale-dependent and tends to zero as the resolution increases; the tensile strength should be infinite, which is meaningless. Finite measures can be obtained only with noninteger (fractal) dimensions. The assumption of the Euclidean domain characterizing the classical continuum theory states that the maximum load F is given by the product of the strength σ_u times the nominal area $A_0 = b^2$. In this model, F equals the product of the Hausdorff fractal measure [38] $A^*_{res} \sim b^{2-d_\sigma}$ of the fractal, like the Sierpinski carpet in Fig. 13a, times the fractal tensile strength σ^*_u [24]:

$$F = \sigma_u A_0 = \sigma^*_u A^*_{res}, \tag{8}$$

where σ^*_u presents the anomalous physical dimensions $[F][L]^{-(2-d_\sigma)}$. The fractal tensile strength is now a true material constant, i.e., it is scale-invariant. From Eq.(8) we obtain the scaling law for tensile strength:

$$\sigma_u = \sigma^*_u b^{-d_\sigma}, \tag{9}$$

i.e., a power law with negative exponent $-d_\sigma$.

Now, let us consider the deformation inside the zone where damage localizes, i.e., within the so-called damaged band. Again, it is possible to assume that the strain field presents fractal patterns. Thus, as representative of the damaged band, consider now a bar subjected to tension (Fig. 13b), where, at the maximum load, dilation strain tends to concentrate into different softening regions, while the rest of the body undergoes elastic unloading. Here, all the quantities refer to tensile properties and therefore we omit the superscript (t) to lessen the notation. Let us assume, for instance, that the strain is localized at cross-sections whose projections onto the longitudinal axis are provided by the triadic Cantor set. The displacement function at rupture can be represented by a Cantor staircase graph, sometimes also called devils staircase (Fig. 13b). The strain defined in the classical manner is meaningless in the singular points, as it diverges. This drawback can be overcome by introducing a fractal strain. Let us indicate with $1 - d_\epsilon$ (where $d_\epsilon \geq 0$) the fractal dimension of the lacunar projection of the damaged sections. According to the fractal measure of the damage line projection, the total elongation w_{cr} of the band at rupture must be given by the product of the Hausdorff measure $b^* \sim b^{1-d_\epsilon}$ of the Cantor set times the critical fractal strain ϵ^*_u, while in the classical continuum theory it equals the product of the length b times the critical strain ϵ_u:

$$w_{cr} = \epsilon_u b = \epsilon^*_u b^{(1-d_\epsilon)}, \tag{10a}$$

$$\epsilon_u = \epsilon^*_u b^{-d_\epsilon}, \tag{10b}$$

where ϵ^*_u has the anomalous physical dimension $[L]^{d_\epsilon}$. The fractal critical strain is the true material constant, i.e., it is the only scale-invariant parameter governing the kinematics of the damaged band. When d_ϵ varies from 0 to 1, the kinematical control parameter w^*_{cr} moves from the canonical critical strain ϵ_u, of dimension $[L]^0$, to the critical crack opening displacement w_{cr}, of dimension $[L]^1$.

Finally, this fractal approach can be applied to the work W necessary to break a concrete specimen of cross section b^2. This work is equal to the product of the fracture energy $\mathcal{G}_F$ times the nominal fracture area $A_0 = b^2$. On the other hand, due to the roughness of the crack surface, which can be modeled as a von Kock surface built on the square of side b, the area A_{dis} diverges as the measure resolution tends to infinity. Therefore, the fracture energy should be zero, which is meaningless. Finite values of the measure of the set where energy is dissipated can be achieved only via noninteger fractal dimension. The fractal dimension of the invasive domain will be $2 + d_{\mathcal{G}}$. In this framework, W equals the product of the fractal Hausdorff measure $A^*_{dis} \sim b^{2+d_{\mathcal{G}}}$ of the rough surface times the fractal fracture energy $\mathcal{G}^*_F$:

$$W = \mathcal{G}_F A_0 = \mathcal{G}^*_F A^*_{dis}, \tag{11a}$$

$$\mathcal{G}_F = \mathcal{G}^*_F b^{d_{\mathcal{G}}}, \tag{11b}$$

where $\mathcal{G}^*_F$ is the true scale invariant material parameter, whereas the nominal value $\mathcal{G}_F$ is subjected to a scale effect described by a power law with positive exponent.

The three size effect laws (9), (10b), and (11b) of the cohesive law parameters are not completely independent of each other. In fact, there is a relation among the scaling exponents that must be always satisfied. This means that, when two exponents are given, the third follows from the first two. In order to get this relation, let us suppose, for instance, to know d_σ and d_ϵ. Generalizing Eqs. (9) and (10b) to the whole softening regime, we get $\sigma = \sigma^* b^{-d_\sigma}$ and $w = \epsilon^* b^{(1-d_\epsilon)}$. These relationships can be considered as changes of variables and applied to the integral definition of the fracture energy:

$$\mathcal{G}_F = \int_0^{w_{cr}} \sigma \mathrm{d}w = b^{1-d_\epsilon-d_\sigma} \int_0^{\epsilon^*_u} \sigma^* \mathrm{d}\epsilon^* = \mathcal{G}^*_F b^{1-d_\epsilon-d_\sigma}. \tag{12}$$

Equation (12) highlights the effect of the structural size on the fracture energy, as Eq.(11b) does. Therefore, comparing Eqs.(12) and (11b), we get the relation among the exponents,

$$d_\sigma + d_\epsilon + d_{\mathcal{G}} = 1. \tag{13}$$

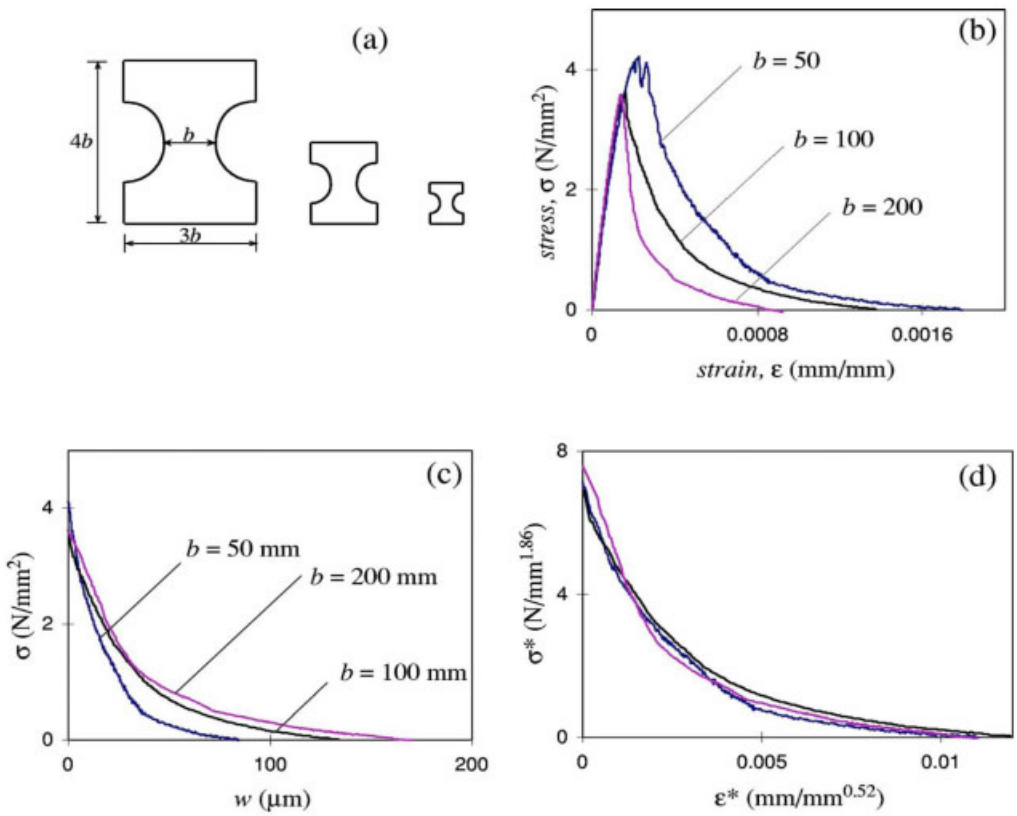

Fig. 14 (online colour at: www.zamm-journal.org) (a) Tensile tests on dog-bone shaped concrete specimens [40]; (b) stress-strain diagrams; (c) cohesive law diagrams; (d) fractal cohesive law diagrams.

Note that, from a physical point of view, the geometrical relationship (12) states that, after the peak load, the energy is dissipated over the infinite lacunar sections where softening takes place inside the damaged band (Fig. 13c).

The fractal fracture energy $\mathcal{G}_F^*$ can be obtained as the area below the fractal softening stress-strain diagram $\sigma^* - \epsilon^*$, according to Eq.(12). Hence, we call the $\sigma^* - \epsilon^*$ diagram the *scale-independent* or *fractal cohesive law*. Contrarily to the classical cohesive law, which is experimentally sensitive to the structural size, this curve should be an exclusive property of the material, being able to capture the fractal nature of the damage process.

This model has been applied to the data obtained from 1994 to 1998 by Carpinteri and Ferro [39, 40] for tensile tests on dog-bone shaped concrete specimens of various sizes under controlled boundary conditions (see Fig. 14).

They interpreted the size effects on the tensile strength and the fracture energy by fractal geometry. Fitting the experimental results, they found the values $d_\sigma = 0.14$ and $d_\mathcal{G} = 0.38$. Some of the $\sigma - \epsilon$ (stress versus strain) and $\sigma - w$ diagrams are reported, respectively, in Figs.14b and 14c, where w is the displacement localized in the damaged band, obtained by subtracting, from the total one, the displacement due to elastic and inelastic pre-peak deformation. Equation (13) yields $d_\epsilon = 0.48$, so that the fractal cohesive laws can be plotted in Fig. 14d. As theoretically expected, all the curves related to the different sizes tend to merge in a unique, scale-independent cohesive law.

An analysis of the data obtained by van Mier and van Vliet [41] according to the fractal cohesive model was also performed in [26]. The results are shown in Fig. 15 and, again, all the curves related to the different sizes tend to merge in a unique, scale-independent cohesive law.

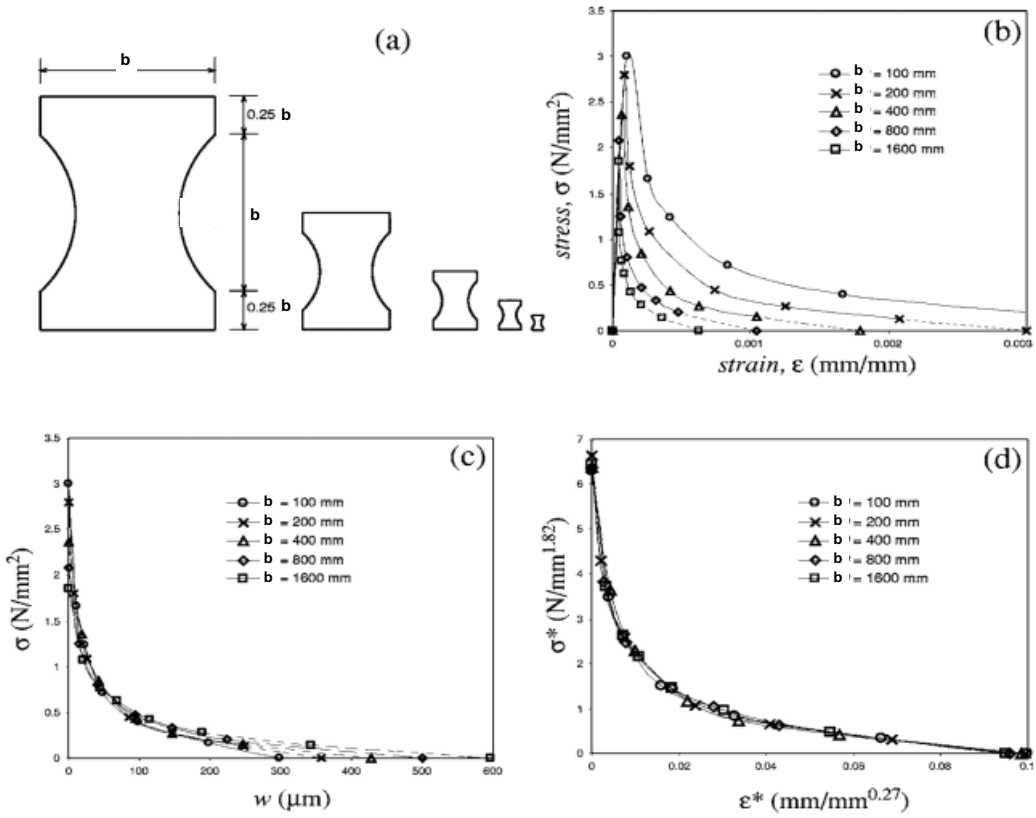

Fig. 15 (a) Tensile tests on dog-bone shaped concrete specimens [41]; (b) stress-strain diagrams; (c) cohesive law diagrams; (d) fractal cohesive law diagrams.

5 Conclusion

The research carried out at the Politecnico di Torino during the last two decades on the modelling of strain localization has been reviewed in the present article. Introducing the elementary cohesive/overlapping zones models in tension/compression, it has been shown that it is possible to get a deep insight into the ductile-to-brittle transition and into the scaling of the material properties of quasi-brittle materials.

A future line of research concerns the applicability and possible generalizations of the cohesive crack model to ductile materials, where the size of the material heterogeneity, i.e., the grain size of polycrystals, is much smaller than the specimen

size considered in standard experimental tests for the determination of fracture parameters of metals. Indeed, size-scale effects are expected to be relevant. The contemporaneous presence of plasticity and discrete cohesive crack propagation increases the modelling complexity. Recent research in this field suggests the possibility to define a *Hardening Cohesive Crack Model* for metallic materials [42]. Moreover, preliminary numerical investigations on the interplay between plasticity and grain boundary decohesion in 2D and 3D polycrystalline materials have been presented in [43]. Further numerical and experimental investigations in this context are expected in the next few years.

References

[1] D. C. Drucker, Some implications of work-hardening and ideal plasticity, Q. Appl. Math. **7**, 411–418 (1950).
[2] T. von Kármán, L. G. Dunn, and H. S. Tsien, The influence of curvature on the buckling characteristics of structures, J. Aero. Sci. **7**, 276–289 (1940).
[3] T. von Kármán and H. S. Tsien, The buckling of thin cylindrical shells under axial compression, J. Aero. Sci. **8**, 303–312 (1941).
[4] D. S. Dugdale, Yielding of steel sheets containing slits, J. Mech. Phys. Solids **8**, 100–114 (1960).
[5] B. A. Bilby, A. H. Cottrell, and K. H. Swinden, The spread of plastic yield from a notch, Proc. R. Soc. Lond. A **272**, 304–314 (1963).
[6] G. I. Barenblatt, The mathematical theory of equilibrium cracks in brittle fracture, Adv. Appl. Mech. **7**, 55–129 (1962).
[7] J. R. Rice, A path independent integral and the approximate analysis of strain concentration by notches and cracks, J. Appl. Mech. **31**, 379–386 (1968).
[8] E. Smith, The structure in the vicinity of a crack tip: a general theory based on the cohesive zone model, Eng. Fract. Mech. **6**, 213–222 (1974).
[9] A. Hillerborg, M. Modeer, and P. E. Petersson, Analysis of crack formation and crack growth in concrete by means of fracture mechanics and finite element, Cem. Concr. Res. **6**, 773–782 (1976).
[10] P. Petersson, Crack Growth and Development of Fracture Zones in Plain Concrete and Similar Materials, Report TVBM-1006, Division of Building Materials (Lund Institute of Technology, Lund, 1981).
[11] A. Carpinteri, Interpretation of the Griffith Instability as a Bifurcation of the Global Equilibrium. In: Application of Fracture Mechanics to Cementitious Composites (Proc. of a NATO Advanced Research Workshop, Evanston, USA, 1984), edited by S. P. Shah (Martinus Nijhoff Publishers, Dordrecht, 1985), pp. 284–316.
[12] A. Carpinteri, Cusp catastrophe interpretation of fracture instability, J. Mech. Phys. Solids **37**, 567–582 (1989).
[13] A. Carpinteri, Decrease of apparent tensile and bending strength with specimen size: two different explanations based on fracture mechanics, Int. J. Solids Struct. **25**, 407–429 (1989).
[14] A. Carpinteri, Post-peak and post-bifurcation analysis on cohesive crack propagation, Eng. Fract. Mech. **32**, 265–278 (1989).
[15] A. Carpinteri, Softening and snap-back instability in cohesive solids, Int. J. Numer. Methods Eng. **28**, 1521–1537 (1989).
[16] Z. Cen and G. Maier, Bifurcations and instabilities in fracture of cohesive-softening structures: a boundary elements analysis, Fatigue Fract. Eng. Mater. Struct. **15**, 911–928 (1992).
[17] M. Elices, G. V. Guinea, and J. Planas, Prediction of Size-Effect Based on Cohesive Crack Model. In: Size-Scale Effects in the Failure Mechanisms of Materials and Structures, edited by A. Carpinteri, (E & FN Spon, London, 1996), pp. 309–324.
[18] M. Elices, G. V. Guinea, J. Gómez, and J. Planas, The cohesive zone model: advantages, limitations and challenges, Eng. Fract. Mech. **69**, 137–163 (2002).
[19] A. Carpinteri, Size effects on strength, toughness and ductility, ASCE J. Eng. Mech. **115**, 1375–1392 (1989).
[20] A. Carpinteri, M. Corrado, M. Paggi, and G. Mancini, Cohesive Versus Overlapping Crack Model for a Size Effect Analysis of RC Elements in Bending. In: Design, Assessment and Retrofitting of RC Structures, Vol. 2 of the Proceedings of the 6th Conference on Fracture Mechanics of Concrete and Concrete Structures (FraMCoS), Catania, Italy, 2007 (Taylor & Francis, London, 2007), pp. 655–663.
[21] A. Carpinteri, M. Corrado, M. Paggi, and G. Mancini, New model for the analysis of size-scale effects on the ductility of reinforced concrete elements in bending, ASCE. J. Eng. Mech. **135**, 221–229 (2009).
[22] A. Hillerborg, Fracture mechanics concepts applied to moment capacity and rotational capacity of reinforced concrete beams, Eng. Fract. Mech. **35**, 233–240 (1990).
[23] A. Pandolfi, S. Conti, and M. Ortiz, A recursive-faulting model of distributed damage in confined brittle materials, J. Mech. Phys. Solids **54**, 1972–2003 (2006).
[24] A. Carpinteri, Fractal nature of material microstructure and size effects on apparent mechanical properties, Mech Mater **18**, 89–101 (1994).
[25] A. Carpinteri, Scaling laws and renormalization groups for strength and toughness of disordered materials, Int. J. Solids Struct. **31**, 291–302 (1994).
[26] A. Carpinteri, B. Chiaia, and P. Cornetti, A scale-invariant cohesive crack model for quasi-brittle materials, Eng. Fract. Mech. **69**, 207–217 (2002).
[27] M. Paggi, Interface Mechanical Problems in Heterogeneous Materials, Ph.D. Thesis (Politecnico di Torino, Torino, 2005).
[28] M. Paggi, A. Carpinteri, and G. Zavarise, A Unified Interface Constitutive Law for the Study of Fracture and Contact Problems in Heterogeneous Materials. In: Analysis and Simulation of Contact Problems, Lecture Notes in Applied and Computational Mechanics, Vol. 27, edited by P. Wriggers and U. Nackenhorst (Springer-Verlag, Berlin, 2006), pp. 297–304.
[29] A. Carpinteri, M. Paggi, and G. Zavarise, Snap-back instability in micro-structured composites and its connection with superplasticity, Strength Fracture Complexity **3**, 61–72 (2005).

[30] A. Carpinteri, G. Lacidogna, and M. Paggi, Acoustic emission monitoring and numerical modelling of FRP delamination in RC beams with non-rectangular cross-section, RILEM Mater. Struct. **40**, 553–566 (2007).
[31] A. Carpinteri, M. Paggi, and G. Zavarise, The effect of contact on the decohesion of laminated beams with multiple microcracks, Int. J. Solids Struct. **45**, 129–143 (2008).
[32] C. Fairhurst, J. A. Hudson, and E. T. Brown, Optimizing the control of rock failure in servo-controlled laboratory test, Rock Mech. **3**, 217–224 (1971).
[33] K. Rokugo, K. Ohno, and W. Koyanagi, Automatical Measuring System of Load-Displacement Curves Including Postfailure Region of Concrete Specimen. In: Fracture Toughness and Fracture Energy of Concrete, International Conference of Fracture Mechanics of Concrete, Lausanne, Switzerland (Elsevier, Amsterdam, 1986).
[34] R. Thom, Structural Stability and Morphogenesis (Benjamin, Reading, Massachusetts, 1975).
[35] C. Bosco and P. G. Debernardi, Experimental investigation on the ultimate rotational capacity of R.C. beams. Report No. 36, Atti del Dipartimento, Politecnico di Torino, Ingegneria Strutturale, (Politecnico di Torino, Torino, 1992).
[36] A. Carpinteri, B. Chiaia, and S. Invernizzi, Three dimensional fractal analysis of concrete fracture at the mesolevel, Theor. Appl. Fract. Mech. **31**, 163–172 (1999).
[37] A. Carpinteri and P. Cornetti, Size effects on concrete tensile fracture properties: an interpretation of the fractal approach based on the aggregate grading, J. Mech. Behav. Mater. **13**, 233–246 (2002).
[38] K. Falconer, Fractal Geometry: Mathematical Foundations and Applications, 2nd ed. (John Wiley, Chichester, 2003).
[39] A. Carpinteri and G. Ferro, Size effects on tensile fracture properties: A unified explanation based on disorder and fractality of concrete microstructure, Mater. Struct. **27**, 563–571 (1994).
[40] A. Carpinteri and G. Ferro, Scaling behaviour and dual renormalization of experimental tensile softening responses, Mater. Struct. **31**, 303–309 (1998).
[41] J. G. M. van Mier and M. R. A. van Vliet, Effect of strain gradients on the size effect of concrete in uniaxial tension, Int. J. Fract. **94**, 195–219 (1999).
[42] A. Carpinteri, B. Gong, and M. Corrado, Hardening cohesive/overlapping zone model for metallic materials: The size-scale independent constitutive law, Eng. Fract. Mech. **82**, 29–45 (2011).
[43] M. Paggi, E. Lehmann, C. Weber, P. Wriggers, and A. Carpinteri, 3D vs. 2D Modelling of Cracking and Plasticity in Polycrystalline Materials. In: Proceedings of the 10th World Congress on Computational Mechanics (WCCM 2012), paper No. 18522 (publ. in press, Brasil, 2012).

